Compressibility Effects in Thin Channels with Injection

G. Balakrishnan,* A. Liñán,† and F. A. Williams‡
University of California, San Diego, La Jolla, California 92093

A theoretical analysis of the inviscid flow between a porous plate and a parallel impermeable plate is performed for small values of the ratio of the plate separation distance to the lateral extent of the plates, for both planar and axisymmetric geometries. The problem of computing the flowfield is reduced to the solution of a single integral equation, which is accomplished numerically. The ratio of specific heats γ is a parameter of the solution, and parametric results are presented from $\gamma = 1.0$ to 1.67. The flow exhibits choking at a critical value of the lateral extent of the plate, in the vicinity of which the Mach number approaches unity. The results are needed in providing external boundary-layer conditions for studying the flame structure in the viscous region between two counterflowing streams when compressibility is important.

Introduction

SUPERSONIC combustion in turbulent mixing layers locally can involve counterflowing streams in which compressibility is important, with the viscous and chemical effects restricted to a narrow layer at the stagnation plane. The outer portions of such counterflows are inviscid and do not experience exothermicity. As a first step toward analyzing the exothermic viscous layer, descriptions are needed of the inviscid counterflow. The present paper provides a solution for a model of the inviscid outer region. The model addresses the flow between a porous plate and a parallel impermeable plate for small values of the ratio of the separation distance between the plates to the lateral extent of the plates. Two such flows can describe the inviscid counterflow, with the viscous layer located at the impermeable plate between them. In addition, laboratory experiments can be designed, involving opposed flow between two porous plates, for studying diffusion-flame combustion under conditions in which compressibility is important. The present analysis provides the external-flow conditions required for the viscous-layer study.

Theoretical analyses of flows between porous plates at high Reynolds numbers began with Proudman's study[1] of an incompressible, nonreacting fluid in a two-dimensional channel with porous walls through which the fluid is injected uniformly. Extensions of this work addressed both heat transfer[2] and combustion[3] in the same type of configuration. The last of these studies was directed toward facilitating quantitative interpretation of results of experimental measurements on counterflow diffusion flames.[4-6] Similar experimental configurations have been employed in much earlier work on linear pyrolysis of vaporizable or decomposable materials, in which steady regression rates were measured when the material was pressed against a heated, impermeable flat plate.[7] The potential importance of compressibility in such experiments has been pointed out by Cantrell,[8] who had earlier[9] completed an analysis of such flows including compressibility effects but not considering the simplifications that arise in the limit of large Reynolds numbers, addressed herein.

Received April 24, 1990; revision received Nov. 2, 1990; accepted for publication Nov. 6, 1990.

*Graduate Student, Department of Applied Mechanics and Engineering Sciences, 9500 Gilman Drive.

†Visiting Professor, Department of Applied Mechanics and Engineering Sciences, 9500 Gilman Drive; permanent address Escuela de Ingenieros Aeronauticos, Ciudad Universitaria, 28040 Madrid, Spain.

‡Fellow, Professor, Department of Applied Mechanics and Engineering Sciences, 9500 Gilman Drive.

Formulation of the Problem

A coordinate system is selected, as shown in Fig. 1, in which the impermeable plate is located at $y = 0$ and the porous plate at $y = h$. The lateral coordinate x runs from $x = 0$ at the stagnation streamline to $x = a$ at the edge of the plates. Velocities in the x and y directions are denoted by u and v, respectively. The injection velocity through the porous plate $V(x)$ will be of order of magnitude V_P, so that $-v$ is of order V_P and u of order $V_P a/h$. Since h/a is a small parameter, $|v/u|$ is small, except near $x = 0$ where u is proportional to x. For small h/a injection Mach numbers must be small, so that compressibility is unimportant near $x = 0$ but can become significant for x of order a, thereby modifying the viscous layer and flame structure in this region. The Reynolds number $Re \equiv V_P h/\nu$ (where ν is the kinematic viscosity) is taken to be large, so that a boundary layer is present on the impermeable plate, but any boundary layer will have been blown off the porous plate. The boundary layer will not be considered here.

Order-of-magnitude estimates show that the transverse pressure differences are of order ρV_P^2, where ρ denotes density, and are small compared with longitudinal pressure differences, which are of order $\rho(V_P a/h)^2$. Therefore, the conservation equations may be taken to be

$$\frac{\partial(\rho u x^k)}{\partial x} + \frac{\partial(\rho v x^k)}{\partial y} = 0 \tag{1}$$

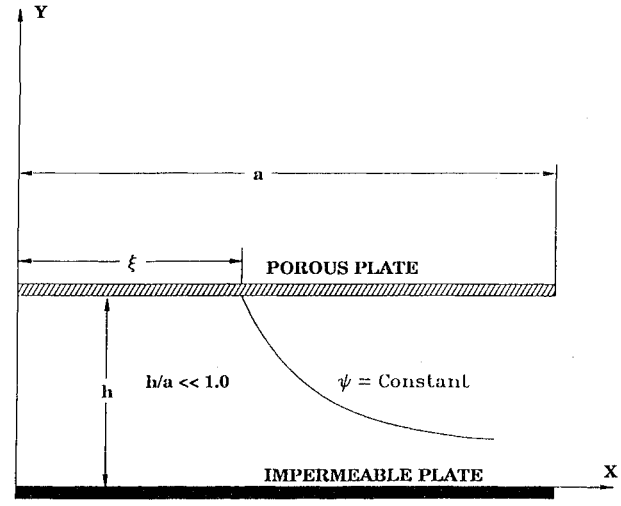

Fig. 1 Schematic representation of the compressible counterflow at high Reynolds numbers.

$$\rho u \frac{\partial u}{\partial x} + \rho v \frac{\partial u}{\partial y} = -\frac{\partial p}{\partial x} \tag{2}$$

$$\frac{\partial p}{\partial y} = 0 \tag{3}$$

$$\rho u \frac{\partial}{\partial x}\left(c_p t + \frac{u^2}{2}\right) + \rho v \frac{\partial}{\partial y}\left(c_p t + \frac{u^2}{2}\right) = 0 \tag{4}$$

where t denotes temperature, c_p the specific heat at constant pressure (assumed constant), and k is zero for planar flows and unity for axisymmetric flows. The simplifications seen in Eqs. (3) and (4) arise from the order-of-magnitude estimates indicated earlier. An ideal gas is considered, so that the pressure is

$$p = \frac{\gamma - 1}{\gamma} c_p \rho t \tag{5}$$

where γ is the ratio of specific heats. An alternative to Eq. (2), derivable from Eqs. (1-5), is

$$\rho u \frac{\partial S}{\partial x} + \rho v \frac{\partial S}{\partial y} = 0 \tag{6}$$

where $S \equiv t/p^{(\gamma-1)/\gamma}$ is a function related to the entropy, which is seen from Eq. (6) to remain constant along streamlines. The boundary conditions for Eqs. (1-4) are

$$u = 0, \quad v = -V(x), \quad t = T(x) \quad \text{at } y = h, \quad 0 \le x < a \tag{7a}$$

$$v = 0 \qquad \text{at } y = 0, \quad 0 \le x < a \tag{7b}$$

$$u = 0, \quad p = p_o \qquad \text{at } x = 0, \quad 0 \le y \le h \tag{7c}$$

where $T(x)$ is the temperature of the porous plate and p_o is the maximum injection pressure at the exit of the porous plate.

The problem defined here is quasiparabolic in that from the equations and boundary conditions the evolution with x of the pressure $p(x)$ and the temperature and velocity profiles $t(x,y)$, $u(x,y)$, and $v(x,y)$ can be determined. No downstream boundary condition in x need be imposed. However, a choking condition at which dp/dx becomes infinite is found to occur at a finite value of x, termed x_c. If $a < x_c$, then $p(a)$ must coincide with the ambient pressure p_a, which thereby determines p_o if $V(x)$ and $T(x)$ are specified independent of $p(x)$. If a is not $< x_c$, then it must coincide with x_c, and $V(x)$ is modified by the choking to achieve this equality. The flow through the porous plate, subject to a given reservoir pressure, must be analyzed to determine the modified $V(x)$. Even for $a < x_c$, the flow through the porous plate may depend on $p(x)$, as considered in a follow-on study that addresses solid-propellant rocket flow,[10] but if the reservoir pressure is sufficiently high and the porosity sufficiently low, this dependence becomes negligible. In the present study, $V(x)$ and $T(x)$ are considered to be given, and the porous plate is not analyzed.

Derivation of the Integral Equation

The independent variables are first transformed from (x,y) to (x,ψ), where the stream function ψ is defined by

$$\psi_y = \rho u x^k, \qquad \psi_x = -\rho v x^k \tag{8}$$

which serves to satisfy Eq. (1). Equations (4) and (6) then imply that

$$t(x,\psi) + u^2(x,\psi)/(2c_p) = T_o(\psi) \tag{9}$$

$$t(x,\psi)/[p(x)]^{(\gamma-1)/\gamma} = S(\psi) \tag{10}$$

where, like S, the stagnation temperature $T_o(\psi)$ is constant along streamlines. There is a one-to-one relationship between ψ and the distance ξ along the porous plate, which is found from Eq. (5), and the second relationship in Eq. (8) to be given by

$$\psi = \left[\left(\frac{\gamma - 1}{\gamma}\right)c_p\right]^{-1} \int_0^{\xi} [x^k V(x) p(x)/T(x)]\,dx \tag{11}$$

It then becomes convenient to transform from (x,ψ) to (x,ξ) as independent variables. Since Eq. (7a) implies that in Eq. (9) $T_o(\psi) = T(\xi)$, Eqs. (9) and (10) take the forms

$$t(x,\xi) + u^2(x,\xi)/(2c_p) = T(\xi) \tag{12}$$

$$t(x,\xi)/[p(x)]^{(\gamma-1)/\gamma} = T(\xi)/[p(\xi)]^{(\gamma-1)/\gamma} \tag{13}$$

respectively. Equations (12) and (13) serve to determine $t(x,\xi)$ and $u(x,\xi)$ in terms of $T(\xi)$ and $p(\xi)$.

Given x and ξ, the coordinate y can be determined by integrating the first relationship in Eq. (8) to obtain

$$y = \int_0^{\psi} \frac{d\psi}{\rho u x^k} = \int_0^{\xi} \left[\frac{t(x,\xi')}{p(x)u(x,\xi')x^k}\right]\left[\frac{\xi'^k V(\xi') p(\xi')}{T(\xi')}\right] d\xi' \tag{14}$$

where Eqs. (5) and (11) have been employed in deriving the last equality. Use of Eqs. (12) and (13) in the last integral gives

$$y = \int_0^{\xi} \left(\frac{\xi'}{x}\right)^k \left[\frac{p(\xi')}{p(x)}\right]^{1/\gamma} \left\{1 - \left[\frac{p(x)}{p(\xi')}\right]^{(\gamma-1)/\gamma}\right\}^{-1/2} \times \frac{V(\xi')\,d\xi'}{\sqrt{2c_p T(\xi')}} \tag{15}$$

Since $\xi = x$ at $y = h$, evaluation of Eq. (15) at $y = h$ provides the integral equation

$$h = \int_0^{x} \left(\frac{\xi}{x}\right)^k \left[\frac{p(\xi)}{p(x)}\right]^{1/\gamma} \left\{1 - \left[\frac{p(x)}{p(\xi)}\right]^{(\gamma-1)/\gamma}\right\}^{-1/2} \frac{V(\xi)\,d\xi}{\sqrt{2c_p Y(\xi)}} \tag{16}$$

After Eq. (16) is solved for $p(x)$, Eq. (15) can be used to calculate $y(x,\xi)$, after which the temperature and velocity profiles are given by Eqs. (13) and (12), in that order.

Nondimensionalization of the Integral Equation and of the Solution

A nondimensional strained coordinate X may be introduced to account for the variations of $V(x)$ and $T(x)$. The new coordinate X is defined by

$$X = \frac{V(0)}{h\sqrt{2[(\gamma-1)/\gamma]c_p T(0)}} \int_0^{x} \frac{V(x')/V(0)}{\sqrt{T(x')/T(0)}}\,dx' \tag{17}$$

Introduction of Eq. (17) into Eq. (16) transforms the integral equation into

$$\sqrt{\frac{\gamma}{\gamma-1}} = \int_0^{x} \left(\frac{\Xi}{X}\right)^k \left[\frac{P(\Xi)}{P(X)}\right]^{1/\gamma} \times \left\{1 - \left[\frac{P(X)}{P(\Xi)}\right]^{(\gamma-1)/\gamma}\right\}^{-1/2} d\Xi \tag{18}$$

where Ξ is defined by Eq. (17) with x replaced by ξ, and $P(X) = p(x)/p_o$. Solving Eq. (18) subject to $P(0) = 1$ will determine the pressure distribution as a function of X. Equation (17) must then be employed to obtain this distribution as a function of x.

The transverse coordinate y will be given as a function of X and Ξ by the transformed form of Eq. (15), namely,

$$\sqrt{\frac{\gamma}{\gamma-1}}\,\frac{y}{h} = \int_0^{\Xi} \left(\frac{\xi'}{x}\right)^k \left[\frac{P(\Xi')}{P(X)}\right]^{1/\gamma} \times \left\{1 - \left[\frac{P(X)}{P(\Xi')}\right]^{(\gamma-1)/\gamma}\right\}^{-1/2} d\Xi' \tag{19}$$

which is integrable directly, prior to determining $x(X)$, only for the planar problem $k = 0$. Equation (19), together with Eqs. (12) and (13), will yield the temperature and velocity profiles after Eq. (18) has been solved to provide $P(X)$. It is convenient to express the velocity profiles in terms of the Mach number $M = u/\sqrt{(\gamma - 1)c_p t}$. The variation of M may be shown according to Eq. (12) to be determined by

$$M^2 = \left(\frac{2}{\gamma - 1}\right)\left[\frac{T(\xi)}{t(x, \xi)} - 1\right] \tag{20}$$

so that Eq. (13) enables M to be calculated from

$$M = \sqrt{\left(\frac{2}{\gamma - 1}\right)\left\{\left[\frac{P(\Xi)}{P(X)}\right]^{(\gamma - 1)/\gamma} - 1\right\}} \tag{21}$$

The procedure will employ Eq. (21) to determine M as a function of x for various values of ξ after Eq. (18) is solved for $p(x)$.

Solution Near the Stagnation Streamline

For small values of X, $P(X)$ is of the form

$$P(X) = 1 - \alpha X^2 + \cdots \tag{22}$$

Substitution of Eq. (22) into Eq. (18) yields the relationship

$$\sqrt{\frac{\gamma}{\gamma - 1}} = \int_0^x \left(\frac{\Xi}{X}\right)^k \left[\left(\frac{\gamma - 1}{\gamma}\right)\alpha(X^2 - \Xi^2)\right]^{-1/2} d\Xi$$

$$= \sqrt{\frac{\gamma}{(\gamma - 1)\alpha}} \int_0^1 \frac{Z^k dZ}{\sqrt{1 - Z^2}} \tag{23}$$

where $Z \equiv \Xi/X$. Equation (23) shows that

$$\alpha = (\pi/2)^2, \qquad k = 0$$

$$= 1, \qquad k = 1 \tag{24}$$

Equation (19) then yields

$$(y/h) = (2/\pi)\sin^{-1}(\Xi/X), \qquad k = 0$$

$$= 1 - \sqrt{1 - (\Xi/X)^2}, \qquad k = 1 \tag{25}$$

in which Eq. (17) was employed in deriving the expression for $k = 1$. By use of Eqs. (22) and (24), the temperature and velocity distributions are found from Eqs. (12) and (13) to be given by

$$t(X, \Xi) = T(\Xi)[1 - (\pi/2)^{2(1-k)}(X^2 - \Xi^2)(\gamma - 1)/\gamma] \tag{26}$$

$$u(X, \Xi) = \sqrt{2[(\gamma - 1)/\gamma]c_p T(\Xi)}(\pi/2)^{1-k}\sqrt{X^2 - \Xi^2} \tag{27}$$

Employment of Eqs. (17) and (25) in the last relationship gives

$$u(x,y) = (\pi/2)V(0)(x/h)\cos[(\pi/2)(y/h)], \qquad k = 0$$

$$= V(0)(x/h)[1 - (y/h)], \qquad k = 1 \tag{28}$$

which coincides with the incompressible solution to the problem.

Equations (22) and (24) are useful for beginning the numerical integration of Eq. (18).

Numerical Integration of the Integral Equation

Since $dP/dX \to \infty$ as $X \to X_c$, improved accuracy in numerical integration is achieved by using P instead of Ξ as the independent variable in Eq. (18), thereby making it easier to deal with singularities in the integrand. Equation (18), therefore, is written as

$$1 = \sqrt{\frac{\gamma - 1}{\gamma}}\int_P^1 \left[\frac{X(P')}{X(P)}\right]^k \left(\frac{P'}{P}\right)^{1/\gamma}\left[1 - \left(\frac{P}{P'}\right)^{(\gamma-1)/\gamma}\right]^{-1/2}$$

$$\times \left[-\frac{dX(P')}{dP'}\right]dP' \equiv \int_P^1 f(P')dP' \tag{29}$$

which is expressed as

$$I_1 + I_2 + I_3 = 1, \qquad I_1 \equiv \int_{P_1}^1 f(P')\, dP'$$

$$I_2 \equiv \frac{\Delta P}{2}\left(f_1 + 2\sum_{\ell=2}^{n-2} f_\ell + f_{n-1}\right), \qquad I_3 \equiv \int_{P_n}^{P_{n-1}} f(P')\, dP' \tag{30}$$

where the step size $\Delta P = P_\ell - P_{\ell+1}$ is taken to be 10^{-3}, and

$$f_\ell = [(\gamma - 1)/\gamma]^{1/2}(X_\ell/X_n)^k(P_n/P_\ell)^{1/\gamma}$$

$$\times [1 - (P_n/P_\ell)^{(\gamma-1)/\gamma}]^{-1/2}(-dX/dP)_\ell$$

according to Eq. (29). Equations (30) show that most of the integral is evaluated by the trapezoidal rule, which results in $I_2 = A_2/X_n^k$, where at each step n the coefficient A_2 is known from the previous $n - 1$ steps. Calculations also were made using Simpson's one-third rule, which enables ΔP to be increased to 10^{-2}, and the same results were then obtained with a substantial saving in computer time. The starting and ending steps, I_1 and I_3, have been split off for separate treatment.

Substitution of Eq. (22) into Eq. (18) and integration, under the approximation that $\alpha\Xi^2 \ll 1$, readily gives, for the I_1 of Eqs. (30), the result that $I_1 = A_1/X_n^k$, where

$$A_1 \equiv [(\gamma - 1)/\gamma]^{1/2}P_n^{-1/\gamma}[1 - P_n^{(\gamma-1)/\gamma}]^{-1/2}$$

$$\times (\Delta P/\alpha)^{(k+1)/2}/(k + 1)$$

which is known from Eqs. (24). To evaluate the I_3 of Eqs. (30), it may be observed that, near $P = P_n$, the first two factors in the integrand in Eq. (29) are nearly unity and the third is approximately

$$\left[\frac{\gamma - 1}{\gamma}\left(\frac{P' - P_n}{P_n}\right)\right]^{-1/2}$$

so that

$$I_3 \approx \int_{P_n}^{P_n + \Delta P} \sqrt{P_n}\frac{dP'}{\sqrt{P' - P_n}}\left(-\frac{dX}{dP}\right)_n$$

$$\approx 2\sqrt{P_n \Delta P}\left(\frac{X_n - X_{n-1}}{\Delta P}\right) \tag{31}$$

which is of the form $A_4X_n - A_3$, where A_3 and A_4 are known. Therefore, the first expression in Eq. (30) can be written as

$$A_4X_n^{k+1} - (1 + A_3)X_n^k + (A_1 + A_2) = 0 \tag{32}$$

from which X_n is readily calculated (by solving a quadratic equation if $k = 1$). Although the linear approximation for the derivative, giving the last equality in Eq. (31), becomes inaccurate as $X \to X_c$, the procedure yielded sufficiently accurate results with the selected step size ΔP.

After $X_n(P_n)$ was calculated as just described, streamlines were obtained, for the case in which $V(x)$ and $T(x)$ are constant (so that $\xi'/x = \Xi'/X$) by evaluating the integral in Eq. (19) numerically. It may be recalled that a streamline corresponds to a constant value of ξ, so that the integral in Eq. (19) to a fixed upper limit for various values of X gives $y(x)$ along the streamline.

Results of the Numerical Integrations

It may be noted that as $\gamma \to 1$ Eq. (18) reduces to

$$1 = \int_0^x \left(\frac{\Xi}{X}\right)^k \frac{P(\Xi)}{P(X)} \frac{d\Xi}{\sqrt{\ell n[P(\Xi)/P(X)]}} \tag{33}$$

which can be solved in the same general manner previously described for Eq. (18). It is for this reason that the factor $(\gamma - 1)/\gamma$ was included before c_p in Eq. (17). In this limit, Eq. (32) becomes

$$M = \sqrt{2\ell n[P(\Xi)/P(X)]} \tag{34}$$

The integration may thus readily be performed for $\gamma = 1$ as well as for other values of γ.

Figures 2 and 3 show $P(X)$ for the axisymmetric and planar flows, respectively. It is seen that all of the curves are qualitatively similar and that choking occurs at $X = X_c$, where P approaches its limiting value P_c with an infinite slope. As γ increases, the value of X_c increases mildly, whereas P_c decreases. Also, X_c is larger and P_c smaller for axisymmetric flows than for planar flows, reflecting the greater relief provided by the increasing area in the axisymmetric geometry. For purposes of comparison, the incompressible solutions from Eqs. (22) and (24) are shown as dashed curves. The incompressible solutions do not exhibit choking. Their initial departures from the compressible solutions have higher pressures at a given value of X for both planar and axisymmetric flows, but Fig. 2 shows that this deviation is exceedingly small for axisymmetric flows and is soon reversed [through the geometrical relief factor (Ξ/X) in Eq. (18)], so that the incompressible solution fortuitously provides a good approximation for the pressure profile all the way to choking, contrary to the two-dimensional behavior seen in Fig. 3.

Figures 4 and 5 exhibit representative streamlines for the axisymmetric and planar flows, respectively, each for a different value of γ. The influence of γ on these streamlines is not too large and is illustrated by a few chain lines drawn in the figures. The expected counterflow field is observed here, except near the choking point, where streamline divergence begins to occur, first at the smaller values of y/h. The divergence is a compressibility effect that leads to a small region of locally supersonic flow, as may be inferred from the curves along which $M = 1$, drawn on these figures. For comparison, a few incompressible-flow streamlines, calculated from Eqs. (25), are drawn as dashed curves in Figs. 4 and 5; these show noticeable departures from the compressible streamlines beginning at about $M = 0.25$.

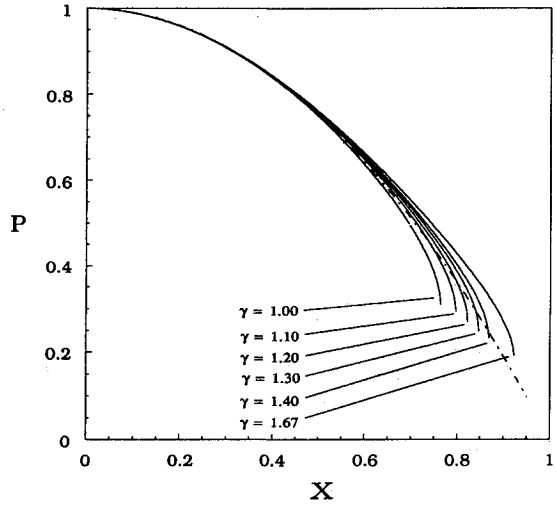

Fig. 2 Variation of pressure ratio with nondimensional distance for the axisymmetric flow configuration and different values of the ratio of specific heats γ (dashed curve for incompressible flow).

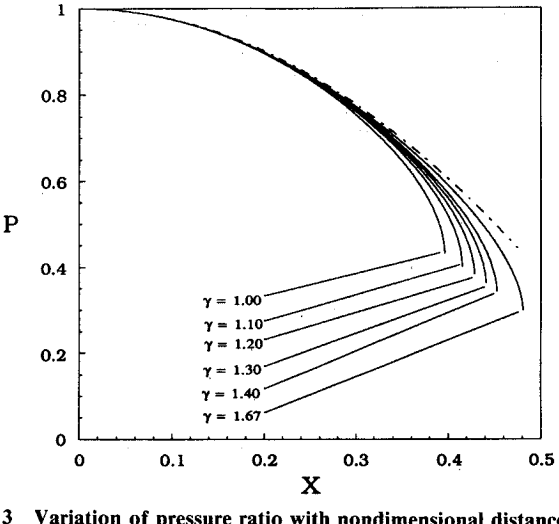

Fig. 3 Variation of pressure ratio with nondimensional distance for the planar flow configuration and different values of the ratio of specific heats γ (dashed curve for incompressible flow).

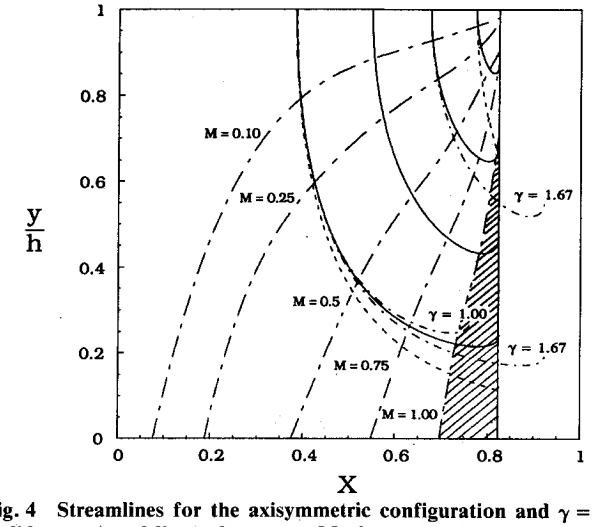

Fig. 4 Streamlines for the axisymmetric configuration and $\gamma = 1.2$ (solid curves) and lines of constant Mach number for this same case (shaded area supersonic); two dashed curves show streamlines for incompressible flow.

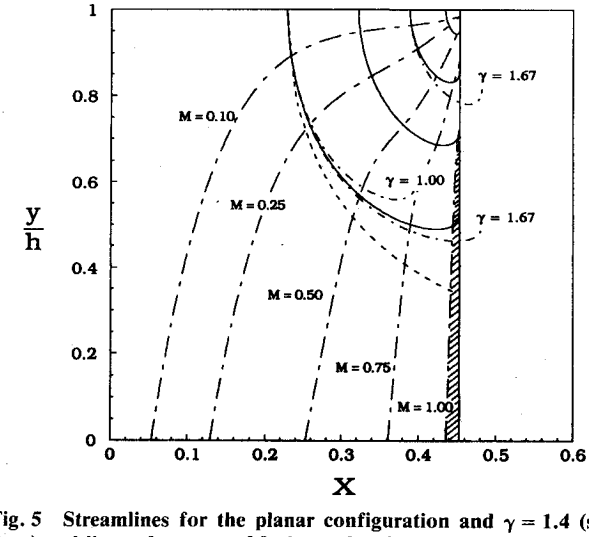

Fig. 5 Streamlines for the planar configuration and $\gamma = 1.4$ (solid lines) and lines of constant Mach number for this same case (shaded area supersonic); dashed curve shows a streamline for incompressible flow.

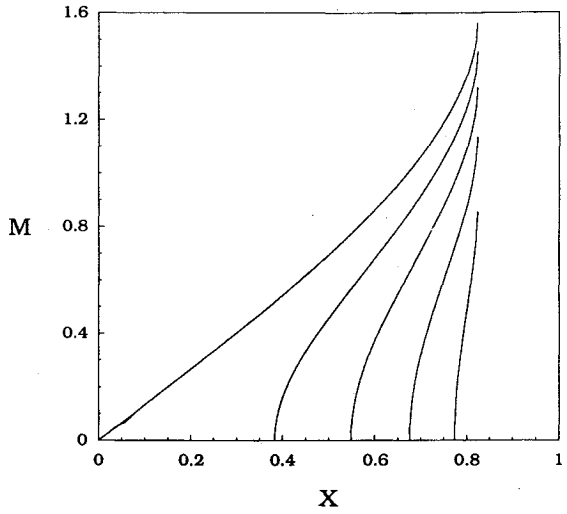

Fig. 6 Variation of Mach number along the streamlines for the axisymmetric flow configuration and $\gamma = 1.2$.

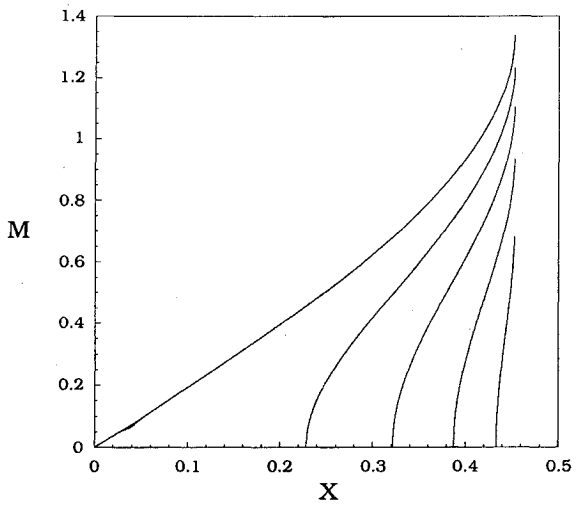

Fig. 7 Variation of Mach number along the streamlines for the planar flow configuration and $\gamma = 1.4$.

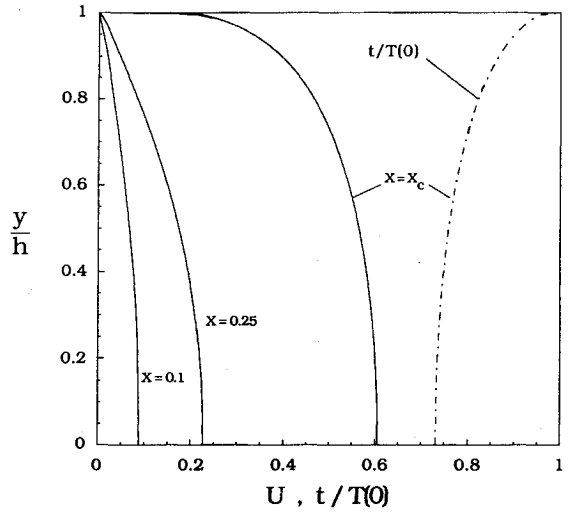

Fig. 8 Velocity profiles $U = u\sqrt{(\gamma-1)c_pT(0)}$ at three different nondimensional streamwise coordinates and the temperature profile $t/T(0)$ at choking for the planar problem with $\gamma = 1.4$.

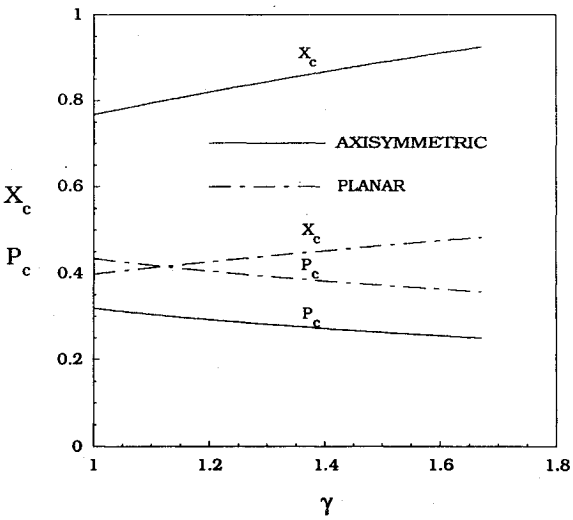

Fig. 9 Dependence of the nondimensional choking distance X_c and choking pressure P_c on the ratio of specific heats γ.

Figures 6 and 7 show representative variations of the Mach number M with X, along selected streamlines, for the axisymmetric and planar flows, respectively. Whereas M increases above unity before choking for streamlines originating near the centerline, it remains below unity for streamlines originating farther toward the edge. The choking condition thus appears to correspond to an average Mach number of about unity. Figure 8 shows representative velocity profiles at various values of X as well as a temperature profile at an extreme case $X = X_c$. The temperature variations are not very large anywhere in the flow. The velocity profile shown at $X = 0.1$ has the cosine form of the incompressible solution given in Eqs. (28), but as choking is approached, it is seen from Fig. 8 that the velocity profiles become much fuller, with steeper gradients at the wall, so that an approximation of incompressible flow would underestimate the skin friction.

Pressure-Field Behavior Near Choking

Curve fitting of the numerical results indicated that near $X = X_c$ the variation of the pressure could be described by

$$P = P_c + \beta\sqrt{X_c - X} \tag{35}$$

where β is a constant. By substituting this form into Eq. (18) and assuming that the major contribution to the integral comes from the vicinity of the upper limit, where the two factors preceding the square root are nearly unity, it is found from expansion of the expression inside the square root that, approximately,

$$1 \approx \int_0^X \left[\frac{\beta}{P_c}(\sqrt{X_c - \Xi} - \sqrt{X_c - X})\right]^{-1/2} d\Xi \tag{36}$$

Introduction of the normalized variables $\eta \equiv X/X_c$ and $\eta' \equiv \Xi/X_c$ into Eq. (36) produces the expression

$$\sqrt{\beta/(P_c X_c^{3/2})} = \int_0^\eta (\sqrt{1-\eta'} - \sqrt{1-\eta})^{-1/2} d\eta' \tag{37}$$

which indicates that

$$\beta = BP_cX_c^{3/2} \tag{38}$$

where B is a constant, independent of all of the parameters of the problem. The results of the numerical integrations are correlated with discrepancies on the order of 1% in P_c by taking $B = 8.35$, so that, in dimensional form, when $V(x)$ and $T(x)$ are constant, Eq. (35) becomes

$$p = p_c\left\{1 + \frac{8.35[V(0)]^2x_c^2}{2[(\gamma-1)/\gamma]c_pT(0)h^2}\sqrt{1-(x/x_c)}\right\} \tag{39}$$

where use has been made of Eq. (17). Equation (39) enables the pressure to be obtained in the vicinity of the choking point when x_c and p_c are known.

The results of the numerical integrations for P_c and X_c as functions of γ are plotted in Fig. 9. These results, which have been discussed in the preceding section, may be used in Eq. (39) to calculate near-choking behavior.

Conclusions and Future Prospects

In the counterflow produced by injection of fluids through two parallel porous plates at high Reynolds numbers, a choking phenomenon occurs at a large lateral extent of the plates. At this choking point, the average Mach number in the inviscid flow reaches a value on the order of unity and compressibility effects are significant. Mach numbers that are large compared with unity, however, are not achievable in this problem. The transverse flow is supersonic only in a small region near the rims of the plates, and only over the central part of this region, in the vicinity of the plane separating the two streams. These results may have bearing on previous linear pyrolysis experiments and on future experiments designed to investigate compressibility effects in counterflow diffusion flames. It may be noted that a supersonic branch also exists, as discussed in subsequent work.[10]

Further studies are needed for investigating possible variations of this flow configuration, for example, in considering effects of pressure matching of the two injected streams when the two fluids and injection conditions differ. The stability of these laminar flow solutions also needs to be considered, although counterflows are known to be relatively stable. Possibilities for nonplanar surfaces separating the two streams should be addressed, with thought given to possibilities for relative area variations leading to transition through choking into high supersonic Mach numbers. In addition, analysis of the structure of the viscous layer separating the two streams is required. The results obtained here provide the boundary conditions needed for this analysis when the pressure matching is consistent with the existence of the planar separation interface. Analyses of diffusion-flame structure and extinction in this boundary layer could help to determine whether the counterflow diffusion flames are more robust near the center or in the wings of the mixing layer.

Acknowledgments

This work was supported by the U.S. Air Force Office of Scientific Research through Grant AFOSR-89-0310. The work of the second author was partially supported by the Spanish CICYT under Grant PB 86-0497.

References

[1]Proudman, I., "An Example of Steady Laminar Flow at Large Reynolds Number," *Journal of Fluid Mechanics,* Vol. 9, 1960, pp. 593–602.

[2]Terrill, R. M., "Heat Transfer in Laminar Flow Between Parallel Porous Plates," *International Journal of Heat and Mass Transfer,* Vol. 8, 1965, pp. 1491–1497.

[3]Seshadri, K., and Williams, F. A., "Laminar Flow Between Parallel Plates with Injection of a Reactant at High Reynolds Number," *International Journal of Heat and Mass Transfer,* Vol. 21, 1978, pp. 251–253.

[4]Kent, J. H., and Williams, F. A., "Extinction of Laminar Diffusion Flames for Liquid Fuels," *Fifteenth Symposium (International) on Combustion,* The Combustion Institute, Pittsburgh, PA, 1975, pp. 315–325.

[5]Seshadri, K., and Williams, F. A., "Effect of CF_3B_2 on Counterflow Combustion of Liquid Fuel with Diluted Oxygen," *ACS Symposium Series No. l6, Halogenated Fire Suppressants,* American Chemical Society, Washington, D.C., 1975, pp. 149–182.

[6]Seshadri, K., and Williams, F. A., "Structure and Extinction of Counterflow Diffusion Flames Above Condensed Fuels: Comparison Between Polymethylmethacrylate and Its Liquid Monomer, both Burning in Nitrogen Air Mixtures," *Journal of Polymer Science,* Vol. 16, 1978, pp. 1755–1778.

[7]Chaiken, R. F., Sibbett, D. H., Sutherland, J. E., Van de Mark, D. K., and Wheeler, A., "Rate of Sublimation of Ammonium Halides," *Journal of Chemical Physics,* Vol. 37, 1962, pp. 2311–2318.

[8]Cantrell, R. H., "Reply by Author to W. H. Andersen," *AIAA Journal,* Vol. 2, 1964, pp. 406–407.

[9]Cantrell, R. H., Jr., "Gas Film Effects in the Linear Pyrolysis of Solids," Ph.D. Dissertation, Harvard University, Cambridge, MA, 1961.

[10]Balakrishnan, G., Liñán, A., and Williams, F. A., "Inviscid Flow in Laterally Burning Solid-Propellant Rocket Motors," Western States Section, The Combustion Institute, Pittsburgh, PA, Paper WSS/CI 90-25, Oct., 1990.